13th International Conference on
Structural Health Monitoring of Intelligent Infrastructure
DOI: 10.3217/978-3-99161-057-1-095

# Post-tensioned wire breaks detection method using distributed acoustic sensing in bridges & viaducts.

Dinesh Lakshmanan [1,2], Felipe Muñoz [1,2], Javier Urricelqui [1], Marco Jimenez-Rodriguez [1]
[1] Uptech Sensing, Pol. Ind. Mutilva Baja, 31192 Mutilva Baja, Navarra, Spain
[2] Universidad Técnica Federico Santa María, Valparaíso, Chile
Email: dinesh.lakshmanan@uptech-sensing.com, felipe.munoz@uptech-sensing.com,
javier.urricelqui@uptech-sensing.com, marco.jimenez@uptech-sensing.com

ABSTRACT: Monitoring the structural integrity of civil infrastructures, such as bridges and viaducts is crucial, as non-visible damage like post-tensioned wire breaks can lead to catastrophic failures, endangering public safety. In this study, we simulate post-tensioned wire breaks by generating controlled mechanical impacts using a sclerometer. These impacts are applied at varying distances from optical fibers cables attached to the tendons of two different structures. A novel detection framework is developed using distributed acoustic sensing (DAS) technology to identify post-tensioned wire breaks in a suspension and a concrete bridge while effectively distinguishing between vehicular noise, environmental noise, and actual wire break events. For suspension bridges, a spectrogram-based template matching approach is implemented, leveraging sub-band selection and image-based analysis to enhance sensitivity to break events while suppressing false positives from environmental noise. In concrete bridges, a deep learning-based convolutional neural network (CNN) model achieves 96% classification accuracy, outperforming traditional methods in detecting wire breaks with high precision. These approaches provide a real-time, reliable solution for structural health monitoring, offering significant advancements in distinguishing critical break events from background interference, improving bridge safety and maintenance strategies.

KEY WORDS: Distributed acoustic sensors, Distributed optical fiber sensors, Structural Health Monitoring, Bridge monitoring

## 1 INTRODUCTION

Bridge maintenance is crucial for infrastructure management, directly impacting public safety and economic stability. Among the key components of bridge structures, post-tensioned cables are essential for enhancing load-bearing capacity and ensuring structural integrity [1]. These high-strength steel tendons, tensioned after concrete curing, play a pivotal role in suspension and concrete bridges. However, wire breaks in post-tensioned systems present a serious risk to structural stability, potentially causing catastrophic failures [2]. Such failures have led to costly repairs and tragic accidents, emphasizing the need for advanced monitoring and detection methods.

Traditional detection methods for wire breaks include techniques such as visual inspections, electromagnetic testing, and strain gauges. While these approaches have served as the foundation for bridge maintenance, they have limitations. Visual inspections are subjective and often miss hidden defects, while electromagnetic testing is hindered by accessibility challenges and the need for specialized equipment [3]. Strain gauges, although effective in measuring tension, lack comprehensive coverage, particularly in inaccessible areas [4]. These limitations highlight the need for real-time, reliable systems for continuous monitoring of bridge infrastructure.

The detection of post-tensioned wire breaks has been investigated using Fiber Bragg Grating (FBG) sensors and acoustic emission (AE) techniques, both crucial for ensuring the structural integrity of bridges and wind turbines. FBG sensors, which are point-based, detect wire breaks by monitoring changes in natural frequency [5], while AE methods, utilizing piezoelectric transducers, capture signals associated with wire fractures [6]. Despite their effectiveness, these approaches face challenges in distinguishing wire break signals from background noise. In contrast, Distributed Acoustic Sensing (DAS) technology presents a promising alternative by converting optical fibers into dense arrays of vibration sensors. DAS sensors offer continuous spatial coverage and capture spatiotemporal patterns, significantly enhancing the detection of wire breaks within noisy environments, particularly in large-scale structures. Additionally, DAS systems enable the tracking of event propagation along the entire length of the optical fiber, a capability absent in point sensors, which are limited to detecting localized signals and cannot monitor the full progression of an event.

DAS technology has emerged as an innovative technology that utilizes fiber optic cables to detect vibrations, enabling real-time data collection and analysis [7]. DAS technology, leveraging optical fibers, is currently used in various applications such as infrastructure monitoring [8], seismic data acquisition[9], security[10], and environmental research[11]. While DAS is typically employed for monitoring natural frequencies in Structural Health Monitoring (SHM)[12], this paper explores its use for detecting potential wire breaks in infrastructure. This technology addresses the shortcomings of traditional methods by providing reliable, continuous monitoring of the entire bridge, allowing for early detection and timely intervention to prevent minor issues from escalating into major problems.

Simulating wire breakages under controlled conditions is essential for thoroughly testing and calibrating the DAS system for detecting such failures. Field testing with actual wire breaks in post-tensioned tendons is inherently challenging and impractical, as it requires the intentional damage of structural elements, which is not a feasible approach for testing.

DOI: 10.3217/978-3-99161-057-1-095

Controlled impact testing has been widely used in structural health monitoring to simulate damage events in prestressed concrete [13], as well as for detecting wire breakages in post-tensioned structures [14]. These methodologies substantiate the use of impact-induced stress waves as a reliable proxy for wire break simulations, enabling repeatable testing without causing irreversible structural damage. To generate these controlled impacts, a sclerometer was utilized, as it is a well-established industry method for producing stress waves that replicate those associated with actual wire failures.

The evolution of detection algorithms for post-tensioned wire breaks using DAS has been driven by the need for efficient and accurate monitoring. Traditional, labor-intensive methods have been replaced by automated systems that employ artificial intelligence, machine learning, and advanced signal processing for real-time detection, even in challenging environments. Although DAS has proven effective in controlled settings, it faces challenges such as external noise and unpredictable conditions [15]. As an example, in railway systems, DAS techniques like gradient analysis and convolution have been used for rail break detection but can struggle with varying track conditions or interference [16].

Machine learning algorithms, such as support vector machines and neural networks, have improved detection accuracy but rely on large, labeled datasets, limiting their effectiveness in dynamic environments [17]. DAS systems have been explored as a promising solution to overcome these limitations in detecting wire breaks in prestressed concrete pipes. For instance, one study introduced a DAS system combined with a pre-trained support vector machine model, achieving 99.62% accuracy in classifying vibrational signals, thus automating the detection process and improving pipeline safety [18]. Another research applied DAS to detect wire breaks by analyzing key parameters, such as zero-crossing rate and short-time energy, which allowed for precise identification and location of acoustic signals generated by wire breaks in large experimental pipelines [19]. While both studies demonstrate the effectiveness of DAS in wire break detection, they do not address other potential causes of structural failure or the influence of environmental factors and external noise, which may limit the accuracy of these systems in practical, real-world settings.

This study proposes a novel approach for detecting post-tensioned wire breaks in bridges using DAS technology. By strategically installing fiber optic cables along post-tensioned tendons, it enables continuous real-time monitoring and advanced signal processing to identify acoustic anomalies indicative of cable failures. This innovative methodology enhances bridge safety, reliability, and maintenance by addressing the limitations of current detection methods. The findings from this research demonstrate the potential of DAS to revolutionize structural health monitoring, offering a more efficient and cost-effective solution for premature failure detection and long-term infrastructure resilience.

## 2 INSTALLATION AND SETUP

An UTS-AS1000 DAS interrogator from Uptech Sensing was employed at two locations: a suspension bridge in Bear Mountain and a viaduct in Florida, both in the United States. A single-sensing optical fiber was used, and measurements were recorded with different fiber installations. The two sites were chosen to evaluate the DAS system's performance in different structural environments.

### *2.1 Installation at Suspension Bridge*

First, in the Bear Mountain suspension bridge installation, the optical fiber was structurally bonded to one of the suspension cables using epoxy resin, enabling distributed acoustic sensing along the cable. A schematic representation of the installation is provided in Figure 1, where the monitored cable is highlighted in red.

Figure 1: Schematic of the optical fiber (red line) installed at Bear Mountain bridge.

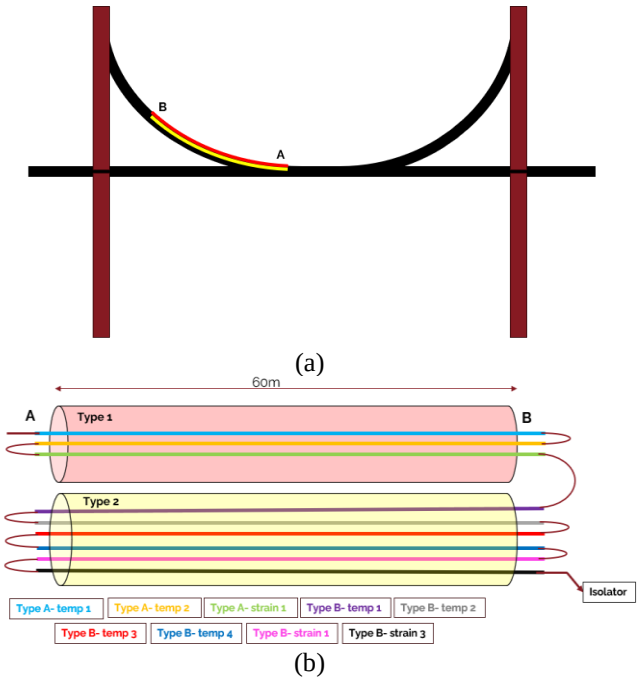


Figure 2: (a) Suspension bridge with fiber optics from Type 1 (red) and Type 2 (yellow) , placed within 1 cm of each other. (b) Fiber arrangement in Type 1(red) and Type 2(yellow) cables with color-coded segments indicating their function.

Two fiber optic cables from different manufacturers were installed in the structure: one from Prysmian (Type 1) and one from Solifos (Type 2), both of them containing several fibers for strain sensing (tight fibers in the cable) and for temperature sensing (loose fibers). The fiber was glued to a suspension cable of the Bear Mountain metal bridge by means of an epoxy

DOI: 10.3217/978-3-99161-057-1-095

resin. These two fibers, strain and temperature, are widely used in industry when measuring with distributed strain and temperature sensors (DTSS), being the first tight bonded, thus sensitive to temperature and mechanical deformations, while the latter loosely bonded, therefore only much less affected by strain variations. However, for DAS sensing, both fibers will detect the acoustic events, since the sensitivity is highly increased with respect to a DTSS, but it is expected to have higher attenuation levels in loose fibers (temperature) rather than in tight fibers (strain).

The schematic representation of the cable installed in the structure is shown in Figure 2(a). Type 1 is highlighted in red, while Type 2 is highlighted in yellow. The Type 1 cable contains three fibers—two temperature-sensitive and one strain-sensitive. The Type 2 cable contains six fibers—four temperature-sensitive and two strain-sensitive. Together, they form a total of nine segments, each of the 60-m-long. The figure drawn is scaled for a better representation of the scenario.

A 540 m composite fiber was formed by fusion-splicing the nine 60 m fiber segments in series. The purpose of creating this composite fiber was to investigate the impact of different fiber couplings on the measurements obtained by the DAS sensor, with the goal of determining whether significant differences in the results could be observed. The splicing at the different ends of fibers A and B is shown in Figure 2(b), with each fiber represented by a distinct color for clarity. In Type 1, the temperature-sensitive fibers are shown in blue and orange, while the strain-sensitive fiber is in green. In Type 2, the temperature-sensitive fibers are represented in purple, gray, red, and blue. The strain-sensitive fibers in Type 2 are shown in pink and black. The figure drawn is scaled for a better representation of the scenario.

After creating the 540 m composite fiber, two distinct cables, each incorporating two different fiber types, were employed to evaluate the performance of both the cables and the optical fibers. The fiber-cable combinations were assessed to evaluate their impact on the system's ability to minimize false positives, improving the reliability of event detection.

### *2.2 Installation at Concrete Bridge*

Next, the interrogator was deployed at the Roosevelt Viaduct in Stuart, Florida, a major highway, where measurements were taken at the second location. It has a twin parallel drawbridge, one for northbound traffic and the other for southbound traffic. The interrogator was connected to a previously installed fiber for DTSS measurements in a road bridge in Florida. The sensing optical fiber is affixed to one of the tendons using an industrial-grade adhesive, ensuring strong coupling for effective vibration and acoustic sensing. This configuration enables the detection of structural responses to environmental and vehicular loads, facilitating distributed acoustic sensing along the bridge.

The optical fiber was installed inside the structure of the Roosevelt Viaduct, with its placement highlighted in red in both images in Figure 3:. In Figure 3:(a), the exterior of the viaduct is shown for reference, providing context for the installation. In Figure 3:(b), the fiber was visibly integrated within the interior, demonstrating its positioning for structural monitoring. This setup was designed to optimize the detection, ensuring effective internal assessment of the viaduct's condition. Additionally, the impacts were generated at different distances from the fiber to evaluate the influence of the distance of the impact from the fiber on the detection performance.

(a)

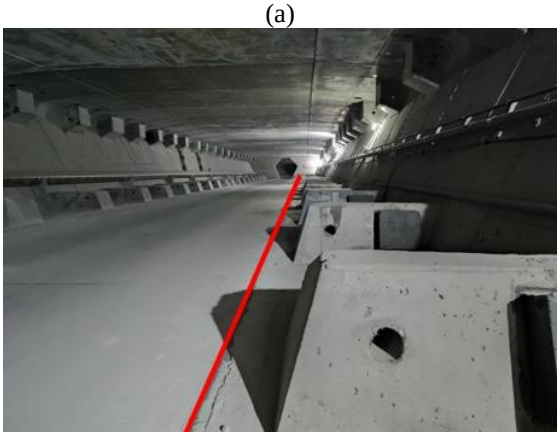

(b)

Figure 3: Optical fiber installation at Roosevelt Viaduct: (a) Exterior perspective from the structure, (b) Interior placement within the structure. Installed fiber is highlighted in red.

Suspension bridges like the Bear Mountain metal bridge rely on cable-supported flexibility, allowing vibrations to dissipate through tensioned cables and the deck, resulting in distributed and oscillatory wave propagation. In contrast, concrete bridges such as the Roosevelt in Florida, with their rigid structural elements, transmit vibrations more directly through the solid slab and supporting components, leading to localized wave reflections and attenuation. This fundamental difference affects how vibrations propagate through each type of bridge[20]. This distinction in vibration behavior underscores the need for tailored monitoring approaches for each bridge type. With this understanding in mind, the impacts on both structures are approached differently.

## 3 WIRE BREAK DETECTION

### *3.1 Experimental Design*

As introduced before, a controlled approach was employed, utilizing a sclerometer to generate impact events, simulating the sound and vibrations generated by a post-tensioned cable break, at varying distances from an optical fiber sensing cable affixed to the tendons of two distinct structures. The study analyzed the DAS system's response to controlled impacts to assess its ability to detect, characterize, and locate potential tendon failures in real-world conditions, while minimizing the possible false cases generated due to other events that might produce similar sound patterns.

DOI: 10.3217/978-3-99161-057-1-095

On one hand, the DAS sensor is configured with a spatial resolution of 2m, a gauge length of 2m, and an acquisition frequency of 2 kHz, monitoring a 540-meter-long optical fiber cable on the suspension bridge installation. On the other hand, for the concrete bridge tests, the system used spatial resolution and gauge length of 3m, with the same acquisition frequency of 2 kHz, to monitor a 3.5-kilometer-long optical fiber.

In the suspension bridge configuration, impact events were generated using a sclerometer to replicate the characteristic waveforms of wire breakage. These impacts were delivered at varying angles relative to the suspension cable axis, enabling the investigation of strike orientation on the propagation of acoustic signals through the structure. As depicted in Figure 4, the monitoring optical fiber, highlighted in red, was positioned along the cable to capture the resulting waveforms. A series of tests was conducted under controlled conditions, with the impact responses systematically recorded for each test. The waveform of the sclerometer hits were obtained for angles of 0º, 45º and 90º with respect to the position of the monitoring fiber. The resulting data were organized into a comprehensive dataset, facilitating further analysis of signal variations as a function of impact direction and intensity.

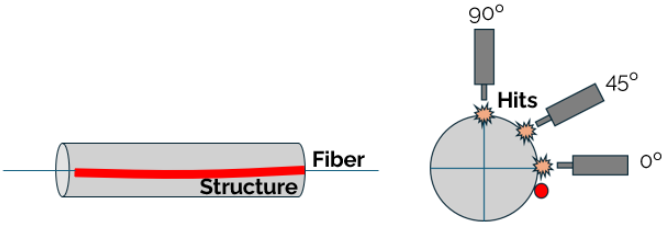


Figure 4: Fiber optic scheme (red line) in suspension cable and sclerometer strike angle diagram relative to the position of the monitoring optical fiber.

For the concrete bridge, impact events were generated at two carefully selected locations to assess the system's sensitivity to structural vibrations. As shown in Figure 5, the sensing fiber highlighted in red was positioned in the concrete slab to capture the resulting waveforms. The first set of impacts was applied at the midpoint of the 19th span, directly on the ground, to simulate the propagation of vibrations through the bridge deck. The second set of impacts was introduced on the ceiling, generating acoustic waves that traversed the upper structural elements. The impact events were generated at varying distances from fiber (0.7112m, 1.4224m, 2.032m, 3.3528m) in both cases. The resulting data were organized into a comprehensive dataset, facilitating further analysis of signal variations as a function of impact direction and intensity.

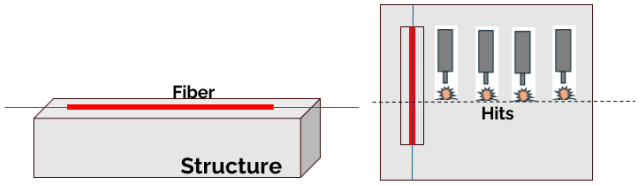


Figure 5: Fiber optic scheme (red line) in concrete slab and sclerometer strike diagram relative to the position of the monitoring optical fiber in the bridge.

### *3.2 Data Analysis*

#### 3.2.1 Data Analysis on Suspension Bridge

Data analysis plays a crucial role in monitoring suspension bridges, enabling the assessment of structural integrity and the identification of potential issues. Nine fiber segments were used to monitor the same region, arranged one after the other in parallel. This configuration results in repeated measurements, with the hit observed across all nine segments. The fiber runs from A to B, as shown in the Figure 2(a) and Figure 2(b).

In this study, the sclerometer hits were obtained for angles of 0º, 45º, and 90º with respect to the position of the monitoring fiber. The waveform of the sclerometer hits was recorded at an angle of 0º relative to the position of the monitoring fiber. Figure 6 presents the first two segments, where the x-axis range from 20 to 80 meters corresponds to the first fiber segment, and the range from 80 to 140 meters represents the second fiber segment. Signal amplitudes are represented by the color scale previously shown, where negative values (down to -2.0 a.u) are indicated by blue hues and positive values (up to 2.0 a.u) are depicted in red, with near-zero values shown in white. All the waterfall plots were generated using this fixed amplitude limit to ensure consistent visual comparison across different events. Distinct diagonal and vertical patterns can be observed in the data distribution.

Two segments monitor the same zone of the suspension cable, and the sclerometer hit was clearly visible in both, characterized by the diagonal pattern. This pattern was attributed to the propagation of the hit made at 0º angle respect to the structure, captured as the disturbance moves through the fiber. Notably, the second segment exhibits a reversed version of the pattern seen in the first segment, which results from the light in the second segment traveling in the opposite direction compared to the first, producing a mirror image of the hit's propagation.

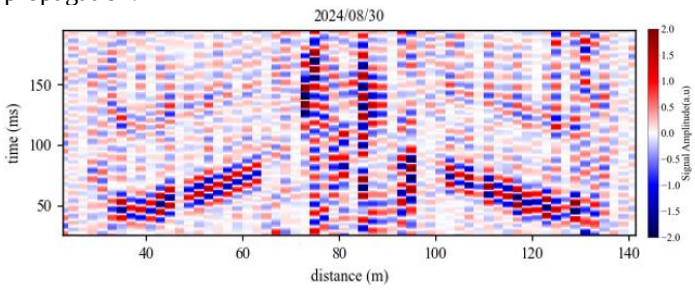


Figure 6: Waterfall data from two segments with the hits from the sclerometer.

Additionally, a fainter hit was observed closer to time 100ms, which was produced by the rebound of the sclerometer hit. It is important to note that whenever a hit is produced, it is usually followed by several rebounds, resulting in the consistent visibility of the secondary, fainter hit. Noise was also observed around the 80-meter mark as a vertical pattern, at the end of cable B, shown in Figure 2(a), is highly susceptible to wind exposure. This noise was not observed at end A, as this portion of the bridge was less affected by winds compared to the other end.

A waterfall diagram containing a sclerometer stroke for the entire length of the fiber is shown in Figure 7. Diagonals with opposite slopes were observed, which were repeated along the

DOI: 10.3217/978-3-99161-057-1-095

spatial axis (x-axis) and were found to correspond to the acoustic signals acquired by the nine optical fiber segments connected in series. Additionally, multiple diagonals over time (y-axis) were identified, representing replicas of the blow that had been generated by the sclerometer.

When comparing the signals acquired from the center of each optical fiber region, it was evident that the strain fibers labeled as "c," "h," and "i" demonstrated the highest sensitivity. This was observed through both temporal and spatial replications, as each of these fibers consistently detected three replicates of the same event at different time intervals and locations. The repeated detection at multiple spatial points and across various times indicates that these fibers were particularly responsive to the transient events, highlighting their effectiveness in capturing the signal. In contrast, the temperature fibers had demonstrated variable sensitivity; fiber "d" had been able to detect the third replication slightly, whereas fibers "a," "b," "e," and "f" had not exhibited such detection capabilities. The consistency of the replicated patterns was observed to indicate a high degree of repeatability in the impact response of the sclerometer. This observation was found to highlight the reliability of strain-sensitive fibers in capturing high-frequency acoustic signals. Moreover, the periodic nature of the detected hits was noted, further reinforcing the consistency of the acquired signals. The temporal waveform at the center of each optical fiber region is presented in Figure 8.

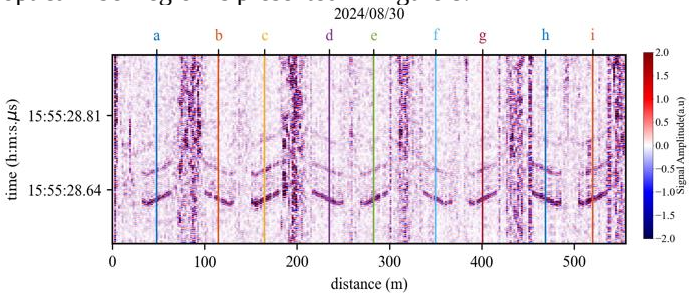


Figure 7: Waterfall diagram showing a sclerometer stroke hits obtained for angles of 0º acquired by the DAS sensor.

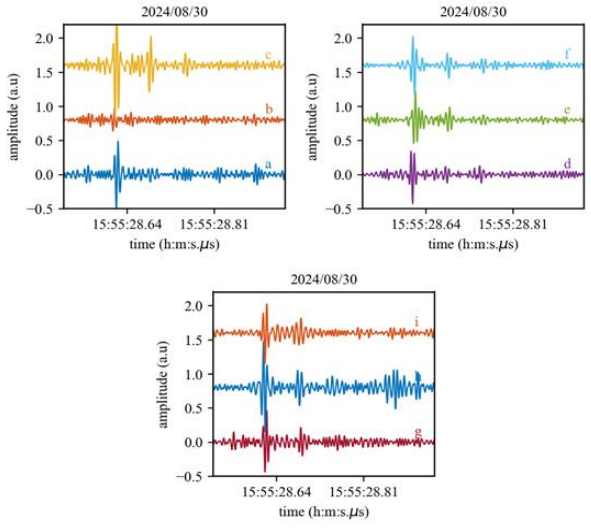


Figure 8: Waveforms at different spatial positions of the monitoring fiber. The spatial positions correspond to those indicated in Figure 7.

The comparison of the performance across the nine segments highlighted distinct differences between fiber types, but no significant differences between cable types. As seen in Figure 8, the strain fibers exhibited a pronounced detection pattern, while the temperature fibers showed a more subtle response. This difference is due to the tight bonding of strain fibers, which makes them highly sensitive to vibrations but also more prone to noise. In contrast, temperature fibers, with their loose bonding, produced less noise but were less effective at detecting vibrations. Therefore, the choice of fiber should depend on the specific application, with strain fibers ideal for high-sensitivity detection and temperature fibers better suited for scenarios where noise reduction is a priority. Additionally, as shown in Figure 7, the detection patterns were consistent across different cables when the same fiber type was used, indicating that cable type had a negligible impact on the overall detection performance.

A similar analysis was conducted for impact angles of 45º and 90º with respect to the cable, revealing variations in the acquired waveforms. At 90º, as shown in Figure 9. The amplitude of the diagonals was observed to be lower than at 0º, and the temporal replicas of the signal could no longer be detected. The corresponding temporal waveform at the center of each optical fiber region, depicted in Figure 10, indicated that the amplitude of the impacts was comparable to background noise, making detection challenging without spatial information.

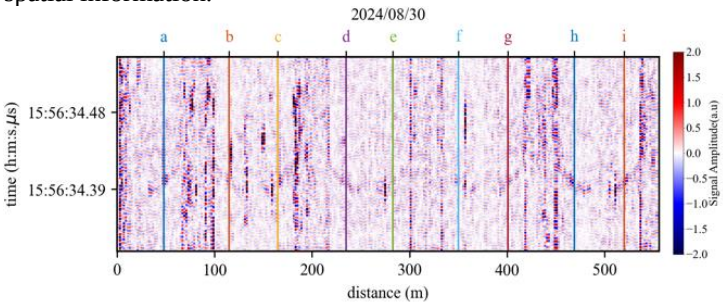


Figure 9: Waterfall diagram showing a sclerometer stroke hits obtained for angles of 90º acquired by the DAS sensor.

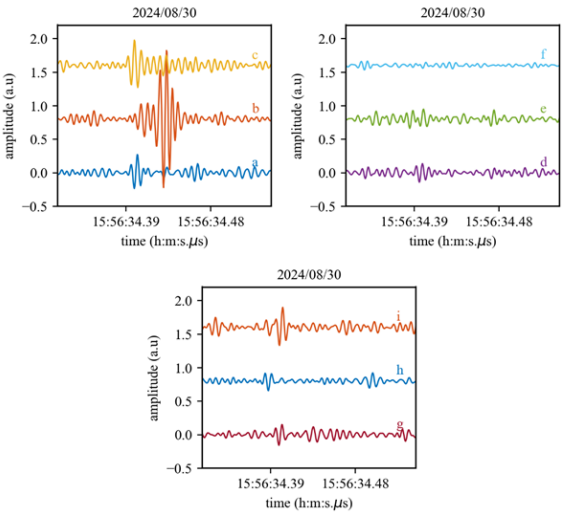


Figure 10: Waveforms at different spatial positions of the monitoring fiber. The spatial positions correspond to those indicated in Figure 9.

DOI: 10.3217/978-3-99161-057-1-095

For the 45º impact, the amplitude of the diagonals, which represents the signal strength along the diagonal axis of the data, as shown in Figure 11, was found to be similar to that of the 0º impact but greater than that of the 90º impact. While temporal replicas were still visible, they appeared significantly attenuated. The temporal waveform at the center of each optical fiber region, presented in Figure 12, demonstrates that the amplitude of the initial impact was distinguishable from noise, whereas the replicas became indistinguishable. These findings indicate that while monitoring fiber effectively captured acoustic events at different impact angles, the detectability of replicated signals was highly dependent on impact orientation, with attenuation effects becoming more pronounced at higher angles.

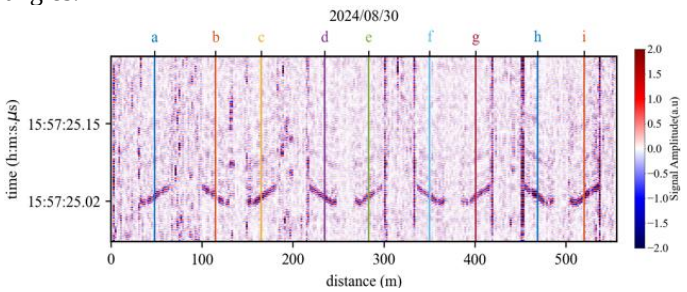


Figure 11: Waterfall diagram showing a sclerometer stroke hits obtained for angles of 45º acquired by the DAS sensor.

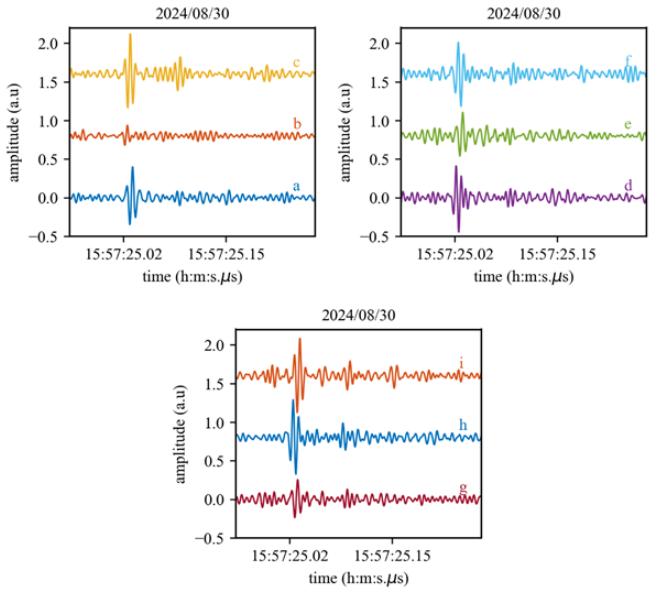


Figure 12: Waveforms at different spatial positions of the monitoring fiber. The spatial positions correspond to those indicated in Figure 11.

The monitoring composite fiber effectively captured acoustic events from different impact angles, although performance depended heavily on the impact orientation. Attenuation effects increased at higher angles, a phenomenon that field experts link to air gaps between the structure and cables at certain orientations, likely caused by installation flaws. Orientations where fibers were closer together experienced less gap interference, resulting in better event detection. This sensitivity profile indicates that high-energy events like tendon ruptures, especially in well-coupled areas, would produce strong, easily detectable signals similar to sclerometer impacts recorded outside poor coupling zones. These findings strengthen the system's potential for reliably detecting critical structural events, boosting confidence in its monitoring ability for vital infrastructure.

### 3.2.2 Data Analysis on the Concrete Bridge

In the context of monitoring concrete bridges, data analysis plays a crucial role in assessing integrity and detecting potential issues. For this analysis, data were recorded from hits generated by a sclerometer, simulating events such as wire breaks. Unlike suspension bridges, where the fiber installation allows for repetition across multiple segments, the configuration of fibers in concrete bridges is unique, meaning repetition of patterns across segments is not expected. A typical hit pattern detected by the interrogator is shown in Figure 13, The pattern clearly shows a hit detected across multiple spatial points, with surface waves propagating from the point of impact to adjacent locations. This wave distribution aids in detecting the event at various points, crucial for assessing the damage's extent.

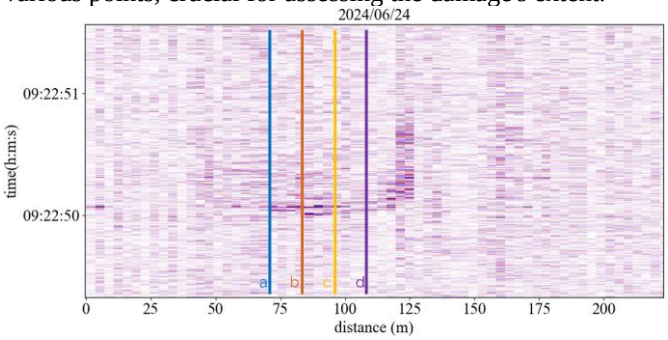


Figure 13: Waterfall diagram showing a sclerometer stroke acquired by the DAS sensor.

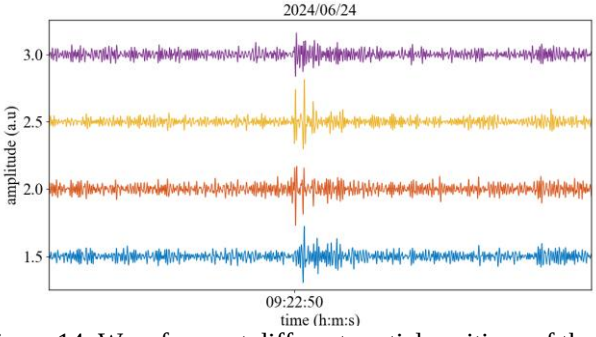


Figure 14: Waveforms at different spatial positions of the monitoring fiber. The spatial positions correspond to those in Figure 13.

A detailed analysis of the acquired signals was conducted, and the temporal waveform at points "a" to "d" was presented in Figure 14. The hits were distinctly observed, and the duration of each blow was measured at approximately the same time 09:22:50. Furthermore, variations in amplitude across different spatial points were identified, suggesting differences in their sensitivity and signal attenuation. The time-domain characteristics of the acquired signals were analyzed, revealing that certain spatial points were more effective at detecting transient events due to their proximity to the point of impact and the propagation of surface waves. It was observed that signals from these locations exhibited stronger and clearer responses. Optimizing fiber selection and positioning could enhance detection accuracy by placing fibers at strategic

DOI: 10.3217/978-3-99161-057-1-095

locations where the signal propagation is most pronounced, thereby capturing more relevant data.

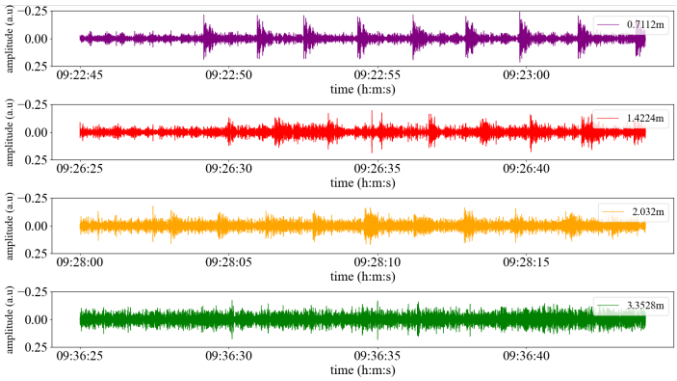


Figure 15: Waveforms at central positions of the fiber monitoring for different hitting lengths from the fiber.

The impacts from the sclerometer at the different distances from the fiber were taken, and the mid spatial point is chosen from all the impacts, and their temporal evolution is shown in Figure 15. The decrease in hit amplitude with increasing depth from the sensor is primarily due to the fundamental principles of seismic wave propagation in concrete. As acoustic waves travel through the slab, their energy disperses, leading to geometric attenuation. Additionally, material absorption within the concrete causes further energy loss. Scattering effects due to variations in the concrete's composition and microstructural heterogeneities also contribute to signal attenuation. These combined factors naturally result in a reduction in amplitude as the distance from the source increases.

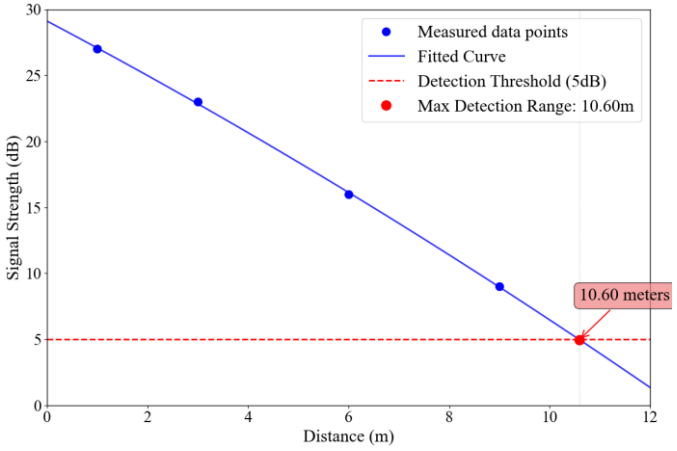


Figure 16 Maximum detection range estimation for tendon break monitoring.

To quantify the effective detection range for tendon break monitoring, the exponential attenuation relationship observed in Figure 15 was extrapolated using curve fitting analysis. The measured signal decay follows $y = ae^{-bx} + c$, with amplitudes decreasing from 27 dB at 1 m to 9 dB at 9 m due to geometric spreading, material absorption, and scattering effects in concrete. A minimum detection threshold of 5 dB was established to ensure reliable discrimination of tendon break signals from background noise. The fitted model, as shown in Figure 16 predicts a maximum effective detection range of 10.6 meters, beyond which the combined effects of wave propagation losses render tendon break detection unreliable. This analysis provides essential parameters for determining sensor spacing in structural health monitoring systems, ensuring complete coverage for the early detection of prestressing tendon failures in concrete bridges.

In conclusion, this analysis highlights the influence of the distance between the sclerometer hits and the fiber on the amplitude of the detected signals. The decrease in hit amplitude with increasing distance is attributed to seismic wave propagation, material absorption, and scattering effects within the concrete. To enhance the sensitivity and reliability of the monitoring system, it is recommended that the sensing fiber be placed closer to the structure, allowing for more accurate detection of breaks and better signal capture.

### *3.3 Detection Algorithm*

#### 3.3.1 Detection Algorithm for Suspension Bridges

The hits from the suspension and concrete bridge were clearly observed in the data, with the temporal traces from the relevant spatial points carefully explored to study the generated impacts. These impacts were analyzed in detail to understand their characteristics and temporal evolution. This was used effectively in designing the detection algorithm for the two structures.

As for the suspension bridge, in this study, a spectrogram-based method was proposed, utilizing only a single fiber segment. A spectrogram-based template matching approach was employed for the suspension bridge to detect transient events in time series data across multiple sensor channels. This method was chosen for its ability to detect transient events across multiple optical fiber segments by leveraging spectrogram-based template matching. The use of multiple optical fiber segments enhances the spatial robustness of the detection, reducing the likelihood of false positives and ensuring reliable identification of events. Additionally, the repetition of results across various fiber segments provides strong validation for detected events, reinforcing the reliability of the method. This approach is preferred over machine learning as it offers a clear, interpretable process that directly correlates spectral energy variations with event detection, without the complexity and data dependency often associated with machine learning models.

The methodology consisted of sequential steps, beginning with spectrogram computation. Given a time series $x(t)$, its time-frequency representation was obtained using the short-time Fourier transform (STFT), producing a spectrogram $S(f,t)$, where $f$ represented frequency and $t$ represented time. For the spectrogram computation, a window length of 256 samples and an overlap of 248 samples were used. This transformation enabled the localization of spectral energy variations over time, forming the basis for subsequent feature extraction.

To enhance sensitivity to specific frequency components, sub-band selection was performed by isolating predefined frequency ranges from the spectrogram. Two sub-bands were defined for analysis: Sub-band 1 ranged from 90 to 180 Hz, and Sub-band 2 ranged from 350 to 440 Hz. This process yielded refined sub-band spectrograms $S'(f,t)$, where only the relevant spectral components were retained. Each extracted sub-band spectrogram was then treated as an image $I(f,t)$ in which pixel

DOI: 10.3217/978-3-99161-057-1-095

intensities corresponded to spectral power. This conversion facilitated the application of image-processing techniques for event characterization.

The core of the detection methodology involved template matching, in which a predefined temporal template was convolved with $I(f,t)$ to identify characteristic signal patterns. The template was designed with three consecutive time slots, where the first and third slots were assigned a weight of -1, and the central slot was assigned a weight of 1. This structure enhanced contrast by emphasizing transient spectral changes while suppressing background variations. The template extended across the entire frequency sub-band, ensuring comprehensive coverage of the targeted spectral range. Through convolution, a response function was obtained that highlighted localized temporal variations indicative of hits.

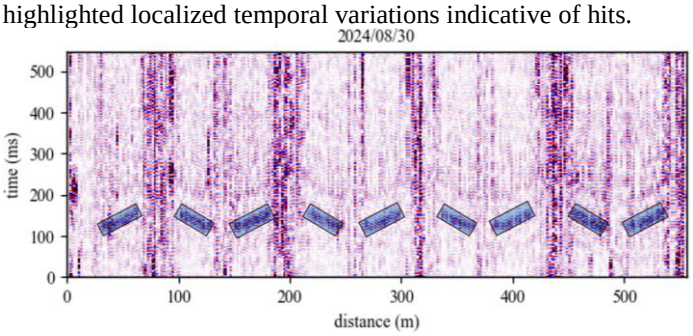


Figure 17: Detection of the hits in the suspension bridge.

To ensure spatial robustness, the template matching procedure was applied independently across multiple fiber sensor locations, generating a three-dimensional response matrix $M(c,t)$ where $c$ represented the sensor channel and $t$ denoted time. Each entry in $M(c,t)$ corresponded to the template matching response at a given location and time. A hit was considered when multiple sensor channels exhibited a significant response simultaneously, thereby reducing the likelihood of false positives caused by localized noise or isolated fluctuations. A thresholding operation was applied to $M(c,t)$ to identify significant activations, ensuring that only strong and spatially correlated events were retained. The detection results are presented in Figure 17, where the significant activations identified through the thresholding operation are distinctly visualized across the sensor channels. The algorithm successfully identified the sclerometer impact points, which are highlighted in pale blue within the figure.

Despite the use of a single segment, minimal false-positive rates were achieved. The analysis was conducted exclusively on this segment, demonstrating the effectiveness of the proposed approach in reducing false positives. These results highlight the spatial and temporal correlations of the detected hits, demonstrating the effectiveness of the method in identifying true events while minimizing false positives. The figure provides a comprehensive overview of the detected impacts within the given time frame and sensor locations. By integrating sub-band selection, image-based template matching, and distributed sensor analysis, the approach provided a scalable and robust solution for detecting transient events in DAS applications. High sensitivity to localized perturbations was achieved while mitigating false positives, making the methodology well-suited for health monitoring and real-time monitoring for the suspension bridge.

### 3.3.2 Detection Algorithm for Concrete Bridges

This study presents a deep learning-based approach for detecting wire breaks in concrete bridges utilizing Convolutional Neural Networks (CNNs). Unlike suspension bridges, which benefit from repetition across multiple segments, allowing for template matching, concrete bridges lack this repeatability in optical fiber segments, necessitating a different method. Machine learning is preferred over traditional techniques because it can automatically learn complex patterns, eliminating the need for manual feature extraction. CNNs are ideal for this task as they efficiently learn complex patterns and features from data, making them highly effective for detecting wire breaks in concrete bridges.

The dataset consists of positive images showing a pattern from hits and negative images of patterns from vehicles and other patterns that are not hits. To generate a more robust dataset for training, a Generative Adversarial Network (GAN) was utilized for data augmentation, as it generated realistic synthetic data that enhanced the training dataset. GAN-based data augmentation techniques were employed here to create additional images, ensuring a larger and more diverse set of training data. The images were preprocessed and resized for uniformity, and the dataset was split into training and testing sets. Positive images were labeled as 1, and negative images as 0. This ensured the model could effectively learn to distinguish between the two classes.

The CNN architecture consists of five fully connected convolutional layers, each followed by a max pooling layer, which reduces the spatial dimensions while retaining key patterns. The number of filters increases progressively with the layers, to capture both low- and high-level features. The extracted feature maps are then flattened and passed through a fully connected layer, followed by a single neuron with a sigmoid activation to classify the images into two categories: breaks (1) or not possible breaks (0).

The training process and the model's learning progression are illustrated in Figure 18, which presents both training and validation loss trends throughout 15 epochs. Two side-by-side plots are shown: the left plot depicts a consistent decrease in loss values for both the training and validation datasets, while the right plot demonstrates an increase in accuracy metrics, which plateaued around 95%. The model was trained efficiently, and convergence was achieved with minimal overfitting, as indicated by the close alignment between validation and training performance throughout the training period.

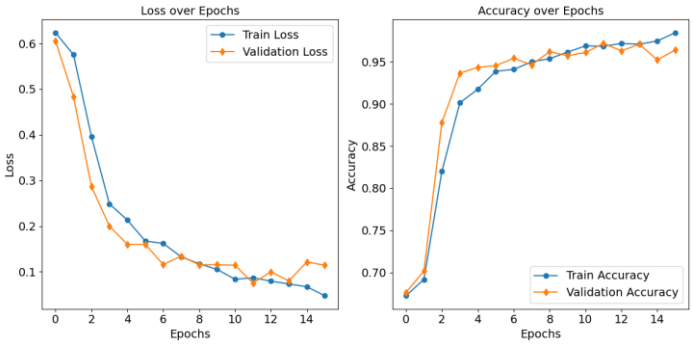


Figure 18 Training and validation loss curves over 16 epochs.

DOI: 10.3217/978-3-99161-057-1-095

Post training, the model's performance was evaluated on the test set, where predictions were converted into binary labels. Standard evaluation metrics, including accuracy, precision, recall, and F1-score, were calculated. Performance metrics and the confusion matrix are presented in Table 1 and the classification report is presented in Table 2, offering a detailed overview of the model's effectiveness. Confidence scores and entropy were also calculated to measure the model's certainty in its predictions.

Table 1 Confusion Matrix

| | Predicted Negative | Predicted Positive |
|---|---|---|
| True Negative | 673 | 19 |
| True Positive | 18 | 313 |

Table 2 Classification Metrics

| Type of Perturbation | Precision | Recall | F-score |
|---|---|---|---|
| Negative | 0.97 | 0.97 | 0.97 |
| Positive | 0.94 | 0.95 | 0.94 |

The predicted labels were visually compared with true labels on a subset of test images to assess the model's accuracy. Based on the results obtained, the proposed deep learning-based model demonstrates robust performance in detecting wire breaks in concrete bridges. The model achieved an overall accuracy of 96%, as evidenced by the confusion matrix and classification report. Visual comparisons of predicted and true labels for a subset of test images highlighted the model's strengths in correctly identifying wire breaks, while also revealing some misclassifications that can be improved. These insights are crucial for refining the model and enhancing its performance. This method's potential to advance structural health monitoring, particularly in the context of bridge inspections, underscores its importance in improving the safety and maintenance of infrastructure.

## 4 CONCLUSION

A comprehensive method was developed for detecting post-tensioned wire breaks in both suspension and concrete bridges using DAS. By tailoring techniques to each bridge type, the approach enabled real-time monitoring and effective detection, classification, and localization of cable break events. These advancements offer valuable applications in improving the safety and maintenance of critical infrastructure.

In the suspension bridge, the monitoring fiber captured acoustic events at various impact angles; however, signal detectability was strongly influenced by orientation. The comparison of performance across different segments revealed distinct differences between fiber types, though no significant differences were observed between cable types. The strain fibers exhibited a pronounced detection pattern, while temperature fibers showed a more subtle response. Based on these findings, a spectrogram-based template matching approach was developed, incorporating sub-band selection and image-based matching. This method enabled accurate detection while maintaining low false positive rates, even when relying on a single fiber segment. Therefore, the choice of fiber should depend on the specific application, with strain fibers ideal for high-sensitivity detection and temperature fibers more appropriate for environments requiring minimal noise.

For the concrete bridge, a decrease in signal amplitude was observed as the distance from the fiber increased. This emphasized the need to place the fiber close to the structural surface. A CNN achieved 96% classification accuracy, outperforming traditional methods in both precision and false positive reduction. Data augmentation using a GAN further improved model generalization by creating a diverse training dataset.

These tailored methodologies provide effective, real-time monitoring strategies for both bridge types. Future efforts should focus on integrating the proposed techniques to improve system accuracy and adaptability in complex environments, and on exploring additional data augmentation strategies to further enhance model robustness.

## FUNDING

This work has been partially funded by the following projects: PTQ2021-011958 Torres Quevedo Grant from Ministerio de Ciencia, Innovación y Universidades, Government of Spain, 0011-1408-2022-000020 and 0011-1408-2023-000026. Doctorados Industriales of 2022 and 2023 from the Government of Navarra.

## REFERENCES

[1] K. D. Bondy and B. Allred, Post-Tensioned Concrete: Principles and Practice, Second Edition, 2nd ed. Boca Raton, FL: CRC Press, 2015.
[2] T. Vogel and S. Fricker, "Condition survey and evaluation of an early post-tensioned bridge verified after removal," Structure and Infrastructure Engineering, vol. 10, no. 3, pp. 359–374, 2013.
[3] M. I. Silva, E. Malitckii, T. G. Santos, and P. Vilaça, "Review of conventional and advanced non-destructive testing techniques for detection and characterization of small-scale defects," Prog. Mater. Sci., vol. 138, p. 101155, 2023.
[4] W. Corte and P. Bogaert, "A case study on strain gauge measurements on large post-tensioned concrete beams of a railway support structure," Insight, vol. 45, pp. 822–826, 2003.
[5] S. Mahmoudkhani, B. Algohi, J. Zhao, H. Ling, A. A. Mufti, and D. J. Thomson, "Acoustic emissions sensor and fuzzy C-mean clustering-based break detection in post-tensioning tendons," IEEE Sensors, 2019.
[6] Xu, R., Lange, A., Käding, M., Ostermann, J., & Marx, S. (2024). Detecting wire breaks in post-tensioned tendons of wind turbines: A signal energy spectrum analysis approach. Proceedings of the 10th European Workshop on Structural Health Monitoring (EWSHM 2024), June 10-13, 2024.
[7] X. Zhang, J. Qi, X. Liang, Z. Guan, Z. Liu, C. Zhang, D. Chen, W. Deng, C. Xu, X. Wang, et al., "Fiber-optic distributed acoustic sensing for smart grid application," Photonics, 2025.
[8] A. Kuttybayeva, A. Abdykadyrov, G. Tolen, A. Burdin, V. Malyugin and D. Kiesewetter, "Application of Distributed Acoustic Sensors Based on Optical Fiber Technologies for Infrastructure Monitoring," 2024 International Conference on Electrical Engineering and Photonics (EExPolytech), Saint Petersburg, Russian Federation, 2024.
[9] M. Li, H. Wang, and G. Tao, "Current and Future Applications of Distributed Acoustic Sensing as a New Reservoir Geophysics Tool," *Open Petroleum Eng. J.*, vol. 8, no. 1, pp. 272-278, 2015.
[10] Ali Masoudi, Gilberto Brambilla; Distributed acoustic sensing with optical fibres: Fundamentals and applications. J. Acoust. Soc. Am. 1 October 2022.
[11] Y. Shang, M. Sun, C. Wang, J. Yang, Y. Du, J. Yi, W. Zhao, Y. Wang, Y. Zhao, and J. Ni, "Research progress in distributed acoustic sensing techniques," Sensors, vol. 22, no. 16, p. 6060, 2022.

DOI: 10.3217/978-3-99161-057-1-095

[12] X. P. Zhang, Y. Y. Shan, Y. H. Zhang, J. Reng, M. M. Chen, and Y. X. Zhang, "An enhanced distributed acoustic sensing system based on the interactions between microstructures," J. Phys. Conf. Ser., vol. 1065, no. 25, p. 252011, 2018.
[13] C. R. Farrar and K. Worden, "An introduction to structural health monitoring," Philos. Trans. A Math. Phys. Eng. Sci., vol. 365, no. 1851, pp. 303–315, Feb. 2007
[14] M. Maizuar, L. Zhang, S. Miramini, P. Mendis, and C. Duffield, "Structural health monitoring of bridges using advanced non-destructive testing technique," in ACMSM25, C. Wang, J. Ho, and S. Kitipornchai, Eds., Lecture Notes in Civil Engineering, vol. 37, Springer, Singapore, 2020.
[15] R. Rueda-García, A. Pérez, and M. López, "Detection of wire break events in prestressed concrete pipes using Distributed Acoustic Sensing systems," *Journal of Structural Engineering*, vol. 150, no. 4, pp. 04023023, Apr. 2024.
[16] A. Wagner, A. Nash, F. Michelberger, H. Grossberger, and G. Lancaster, "The effectiveness of distributed acoustic sensing (DAS) for broken rail detection," Energies, 2023.
[17] M. Bublin, "Event detection for distributed acoustic sensing: Combining knowledge-based, classical machine learning, and deep learning approaches," Sensors, vol. 21, no. 22, p. 7527, 2021.
[18] T.-Y. Zhang, C.-C. Zhang, B. Shi, Z. Chen, X. Zhao, and Z. Wang, "Artificial intelligence-based distributed acoustic sensing enables automated identification of wire breaks in prestressed concrete cylinder pipe," Journal of Applied Geophysics, Apr. 2024.
[19] L. Rueda-García, D. Tasquer-Val, P. Calderón-Bofías, and P. A. Calderón, “Detecting wire breaks in prestressed concrete pipes: an easy-to-install distributed fibre acoustic sensing approach,” Structural Health Monitoring-an International Journal, Mar. 2024.
[20] N. J. Gimsing and C. T. Georgakis, Cable Supported Bridges: Concept and Design, 3rd ed. Chichester, UK: John Wiley & Sons, 2012.